Eur. Phys. J. C 18, 393–403 (2000)
Digital Object Identifier (DOI) 10.1007/s100520000507

THE EUROPEAN PHYSICAL JOURNAL C

Scales, couplings revisited and low-energy phenomenology in M-theory on S^1/Z_2

Chao-Shang Huang[1], Tianjun Li[2], Wei Liao[1], Qi-Shu Yan[1,3], Shou Hua Zhu[1,4]

[1] Institute of Theoretical Physics, Academia Sinica, P.O. Box 2735, Beijing 100080, P.R. China
[2] Department of Physics, University of Wisconsin, Madison, WI 53706, USA
[3] Department of Physics, Tsinghua University, Beijing 100084, P.R. China
[4] CCAST (World Lab), P.O. Box 8730, Beijing 100080, P.R. China

Received: 9 June 1999 / Revised version: 12 July 2000 /
Published online: 27 November 2000 – © Springer-Verlag 2000

Abstract. We reconsider the dimension-11 Planck scale, the physical scale of the eleventh dimension, the physical scale of the Calabi–Yau manifold and the coupling in the hidden sector in M-theory on S^1/Z_2. Also we discuss reasonable bounds on them. Considering the F-term of the dilaton and moduli SUSY breaking and choosing two representative points which correspond to the scalar quasi-massless scenario and the dilaton dominant SUSY breaking scenario, respectively, we analyze experimental constraints on the parameter space. The sparticle spectrum and some phenomenological predictions are also given.

1 Introduction

In recent years revolutionary progress in our understanding of string theories has been made. The key discoveries were dualities, which show that the five distinct superstring theories are in fact five different perturbative expansions of a single underlying theory (11-dimensional M-theory or 12-dimensional F-theory) about five different points in the moduli space of consistent vacua. The dualities, furthermore, show that in addition to the five points of the moduli space, there is a sixth special point in the moduli space which involves an 11-dimensional Minkowski space-time and is related to the strongly coupled heterotic (HE) and IIA superstring theories by compactifications on S^1/Z_2 and S^1, respectively [1]. Nowadays we do not have a complete picture of M-theory so that one might argue that it is premature to make any attempt at phenomenology. However, our experience in investigating weakly coupled $E_8 \times E_8'$ HE superstring phenomenology tells us that it may be that the corners of the moduli space capture most of the features of the theory relevant for low-energy phenomenology.

Since Horava and Witten [2] described the strongly coupled $E_8 \times E_8'$ HE string theory by M-theory compactified on S^1/Z_2 whose low-energy limit is the 11-dimensional supergravity, many interesting implications for the phenomenology have been studied: Newton's constant and compactification, gluino condensation and supersymmetry breaking, axions and the strong CP problem, the threshold scale and strong coupling effects, proton decay, and phenomenological consequences [3–26] (for a review, see [27]). In short, all of the above results seem to show that M-theory is a better candidate than the previous weakly coupled heterotic string theory.

The most important discovery in M-theory phenomenology is that the discrepancy between the grand unification scale of around 2×10^{16} GeV estimated by extrapolating from the LEP measurements and the estimate of around 4×10^{17} GeV calculated in the weakly coupled $E_8 \times E_8'$ HE string theory may be removed in the strongly coupled $E_8 \times E_8'$ HE string theory. In Horava and Witten's picture, at one end of the 11th dimensional line segment of length $\pi\rho$ live the observable fields contained in E_8, at the other end live the hidden sector fields contained in E_8', and in the middle ("bulk") propagate the gravitational fields. One further needs to consider $R_4 \otimes X_{\rm CY}$ ($X_{\rm CY}$ denotes a 6-dimensional Calabi–Yau manifold) compactification of the 10-dimensional $E_8 \times E_8'$ HE string in order to get a realistic effective theory. Therefore, there are several scales and couplings such as the dimension-11 Planck scale, the physical scale of the eleventh dimension, the physical scale of the Calabi–Yau manifold and the couplings in the observable and hidden sectors. The values of these scales and couplings and the relations between them have been estimated [3,12,15].

Because the values of the scales and couplings are important for the phenomenology and there are some issues which need to be discussed, in this paper we shall first reconsider the dimension-11 Planck scale, the physical scale of the eleventh dimension, the physical scale of the Calabi–Yau manifold and the coupling (in terms of the function x which is defined by $x = (\alpha_{\rm H}\alpha_{\rm GUT}^{-1} - 1)/(\alpha_{\rm H}\alpha_{\rm GUT}^{-1} + 1)$) in the hidden sector in M-theory on S^1/Z_2 in standard embedding and non-standard embedding [23–26], and then

discuss the possible bounds on them from the ansatz that the dimension-11 Planck scale is larger than the $M_{\rm GUT}$, $M_{\rm H}$ which is the scale in the hidden sector just after the Calabi–Yau manifold is compactified, the eleventh dimension scale being $[\pi\rho_{\rm p}]^{-1}$. For the standard embedding, we obtain that the upper bound on x is 0.97 ($x < 0.97$), for $\alpha_{\rm GUT} = 1/25$.

An important scale which is directly relevant to phenomenology is the scale $\Lambda_{\rm SUSY}$ from which the soft terms start running. There is a significant difference for $\Lambda_{\rm SUSY}$ between the weakly coupled and strongly coupled limits. In the weakly coupled limit $\Lambda_{\rm SUSY}$ is close to $M_{\rm Pl}$ since observable and hidden sector fields as well as gravitational fields all live in a same 10-dimensional space-time. In the strongly coupled limit, as Horava [4] has argued, SUSY breaking is not felt immediately in the observable sector because of a topological obstruction (the 11th dimension separates the two sectors). SUSY breaking in the hidden sector communicates to the observable sector by gravitational interactions. Therefore, SUSY breaking in the observable sector becomes apparent only after the renormalization scale Q is low enough not to reveal the presence of the 11th dimension anymore. Therefore, a natural and reasonable choice is $\Lambda_{\rm SUSY} = [\pi\rho_{\rm p}]^{-1}$. We estimate the value of $[\pi\rho_{\rm p}]^{-1}$ and get for a lower bound on it 9.5×10^{13} GeV.

In order to discuss the M-theory low-energy phenomenology, we may need to pay attention to the supersymmetry breaking in M-theory and think about M-theory model building (essentially compactifications of 6-dimensional space-time), which is similar to what happened 10 years ago. As we know, we can discuss the supersymmetry breaking in the following ways: non-zero F-terms of the dilaton or moduli fields SUSY breaking in which we do not specify the trigger of the SUSY breaking [15,18,19], and the Scherk–Schwarz mechanism on the eleventh (or fifth) dimension (or we might call it coordinate-dependent compactification) [8,9]. In this paper we consider the phenomenology in non-zero F-terms of the dilaton and/or moduli SUSY breaking.

From the phenomenological view, the important features of M-theory phenomenology which are different from the weakly coupled limit and independent of the details of M-theory model building concern unification of the couplings and the magnitude of $\Lambda_{\rm SUSY}$ and the emphasis of this paper is on investigating the characteristic features of low-energy phenomenology of M-theory. In this paper, we take the simplest compactification as an example (like most people did) and choose two representative points which correspond to the scalar quasi-massless scenario and dilaton dominant SUSY breaking scenario, respectively. Then we calculate the low-energy sparticle spectrum under the LEP experiment constraints and discuss its dependence on $\Lambda_{\rm SUSY}$. It is found that $M_{1/2}$ cannot be larger than 400 GeV if one demands that masses of sparticles are not beyond 1 TeV. We analyze the constraints to the parameter space from $b \to s\gamma$. It is found that in the dilaton dominant SUSY breaking scenario although $b \to s\gamma$ imposes stringent constraints to the parameter space, there still is a region of the parameter space where $\tan\beta$ is large and $M_{1/2}$ is small, which will lead to significant SUSY effects in some processes.

In this paper, we discuss the scales and couplings in the Sect. 2. In Sect. 3, we discuss soft terms. In Sect. 4 we calculate the sparticle spectrum using revised ISAJET. Section 5 is devoted to an analysis of the constraints from $b \to s\gamma$. We discuss the rare decay $B \to X_s\tau^+\tau^-$ and the search for Higgs bosons in Sect. 6. Finally, Sect. 7 contains our conclusion.

2 Eleventh dimension scale and gauge coupling in the hidden sector

First, let us consider the gauge couplings, gravitational coupling and the physical eleventh dimension radius in the M-theory. The relative 11-dimensional Lagrangian is given by [2]

$$L_B = -\frac{1}{2\kappa^2}\int_{M^{11}} {\rm d}^{11}x\sqrt{g}R - \sum_{i=1,2}\frac{1}{2\pi(4\pi\kappa^2)^{2/3}}\int_{M_i^{10}} {\rm d}^{10}x\sqrt{g}\frac{1}{4}F^a_{AB}F^{aAB}. \quad (1)$$

In the 11-dimensional metric[1], the gauge coupling and gravitational coupling in dimension-4 are [3,12]

$$8\pi G_N^{(4)} = \frac{\kappa^2}{2\pi\rho_{\rm p}V_{\rm p}}, \quad (2)$$

$$\alpha_{\rm GUT} = \frac{1}{2V_{\rm p}(1+x)}(4\pi\kappa^2)^{2/3}, \quad (3)$$

$$[\alpha_{\rm H}]_W = \frac{1}{2V_{\rm p}(1-x)}(4\pi\kappa^2)^{2/3}, \quad (4)$$

where x is defined by

$$x = \pi^2\frac{\rho_{\rm p}}{V_{\rm p}^{2/3}}\left(\frac{\kappa}{4\pi}\right)^{2/3} \times \int_X \omega\wedge\frac{{\rm Tr}F\wedge F - \frac{1}{2}{\rm Tr}R\wedge R}{8\pi^2}, \quad (5)$$

where $\rho_{\rm p}$, $V_{\rm p}$ are the physical eleventh dimension radius and Calabi–Yau manifold volume (which is defined by the middle point Calabi–Yau manifold volume between the observable sector and the hidden sector) respectively, and $V_{\rm p} = Ve^{3\sigma}$ where V is the internal Calabi–Yau volume (for details, see [12]).

From the above formula, we obtain

$$x = \frac{\alpha_{\rm H}\alpha_{\rm GUT}^{-1} - 1}{\alpha_{\rm H}\alpha_{\rm GUT}^{-1} + 1}. \quad (6)$$

The GUT scale $M_{\rm GUT}$ and the hidden sector scale $M_{\rm H}$ when the Calabi–Yau manifold is compactified are

$$M_{\rm GUT}^{-6} = V_{\rm p}(1+x), \quad (7)$$

[1] Because we think that the 11-dimensional metric is more fundamental than the string metric and the Einstein frame, we discuss the scales and couplings in 11-dimensional metric

$$M_{\rm H}^{-6} = V_{\rm p}(1-x), \tag{8}$$

or we can express the $M_{\rm H}$ as

$$M_{\rm H} = \left(\frac{\alpha_{\rm H}}{\alpha_{\rm GUT}}\right)^{1/6} M_{\rm GUT} = \left(\frac{1+x}{1-x}\right)^{1/6} M_{\rm GUT}. \tag{9}$$

Noticing that $M_{11} = \kappa^{-2/9}$, we have

$$M_{11} = \left[2(4\pi)^{-2/3}\alpha_{\rm GUT}\right]^{-1/6} M_{\rm GUT}. \tag{10}$$

We can also obtain the physical scale of the eleventh dimension in the 11-dimensional metric:

$$[\pi\rho_{\rm p}]^{-1} = \frac{8\pi}{1+x}\,(2\alpha_{\rm GUT})^{-3/2}\,\frac{M_{\rm GUT}^3}{M_{\rm Pl}^2}. \tag{11}$$

Now, we consider the constraints. Our ansatz is that the scale of $M_{\rm GUT}$, $M_{\rm H}$ and $[\pi\rho_{\rm p}]^{-1}$ should be lower than the 11-dimensional Planck scale. From the constraints that $M_{\rm GUT}$ and $M_{\rm H}$ be smaller than the scale of M_{11}, we obtain

$$\alpha_{\rm GUT} \le \frac{(4\pi)^{2/3}}{2}, \quad \alpha_{\rm H} \le \frac{(4\pi)^{2/3}}{2}, \tag{12}$$

or

$$\alpha_{\rm GUT} \le 2.7, \quad \alpha_{\rm H} \le 2.7; \tag{13}$$

these are independent numbers and they are large enough for our discussion. For the standard embedding, we obtain that the upper bound on x is 0.97 ($x < 0.97$), for $\alpha_{\rm GUT} = 1/25$.

From the constraint that $[\pi\rho_{\rm p}]^{-1}$ is smaller than the scale of M_{11}, we obtain

$$M_{\rm GUT}\alpha_{\rm GUT}^{-2/3} \le \sqrt{1+x}\,2^{1/6}(4\pi)^{-4/9} M_{\rm Pl}, \tag{14}$$

which is obviously satisfied for standard embedding. However, if we consider the non-standard embedding $x < 0$ [23–26], i.e., the gauge coupling in the observable sector is larger than the coupling in the hidden sector, we will have the following lower bound on x:

$$x_{\rm lb} \ge 2^{-1/3}(4\pi)^{8/9}(\alpha_{\rm GUT})^{-4/3}\frac{M_{\rm GUT}^2}{M_{\rm Pl}^2} - 1. \tag{15}$$

Therefore, there exist three possibilities between the physical scale of the eleventh dimension and the physical scale of the Calabi–Yau manifold: $[\pi\rho_{\rm p}]^{-1}$ is smaller than $M_{\rm GUT}$ and $M_{\rm H}$ which, from low energy to high energy, corresponds to the range from dimension-4 to dimension-5 and then, to dimension-11; $[\pi\rho_{\rm p}]^{-1}$ is smaller than $M_{\rm GUT}$ but larger than $M_{\rm H}$, which, assuming x^{11} is the coordinate of the eleventh dimension, and the observable sector is at $x^{11} = 0$ plane and the hidden sector at $x^{11} = \int {\rm d}x^{11}\,(g_{11,11})^{1/2}$ or the opposite plane, from low energy to high energy, corresponds at one particular point x_c^{11}, to the range from dimension-4 to dimension-11 directly, for $x^{11} < x_c^{11}$, from dimension-4 to dimension-5 and then, to dimension-11, and for $x^{11} > x_c^{11}$, from dimension-4 to dimension-10 and then, to dimension-11; $[\pi\rho_{\rm p}]^{-1}$ is larger than $M_{\rm GUT}$ and $M_{\rm H}$ which, from low energy to high energy, corresponds to the range from dimension-4 to dimension-10 and then, to dimension-11. Let us define the $x_{\rm H}$ and x_O which correspond to $[\pi\rho_{\rm p}]^{-1} = M_{\rm H}$ and $[\pi\rho_{\rm p}]^{-1} = M_{\rm GUT}$, respectively. We write

$$\left[\frac{(1+x_{\rm H})^7}{1-x_{\rm H}}\right]^{1/6} = 8\pi(2\alpha_{\rm GUT})^{-3/2}\frac{M_{\rm GUT}^2}{M_{\rm Pl}^2}, \tag{16}$$

$$x_O = 8\pi(2\alpha_{\rm GUT})^{-3/2}\frac{M_{\rm GUT}^2}{M_{\rm Pl}^2} - 1. \tag{17}$$

It is obvious from (11) that when x decreases, $[\pi\rho_{\rm p}]^{-1}$ increases if we consider a specific $\alpha_{\rm GUT}$ and $M_{\rm GUT}$, so we have $x_{\rm H} \ge x_O \ge x_{\rm lb}$.

Now we can discuss the numerical result. We take $M_{\rm GUT} = 2.0 \times 10^{16}\,{\rm GeV}$, $\alpha_{\rm GUT} = 1/25$, $M_{\rm Pl} = 2.4 \times 10^{18}\,{\rm GeV}$; then we obtain $M_{11} = 4.04 \times 10^{16}\,{\rm GeV}$, $x_{\rm lb} = -0.96$, $x_O = -0.92$. Next we have $x_{\rm H} = -0.878$, $[\pi\rho_{\rm p}]^{-1}$ goes from $7.8 \times 10^{14}\,{\rm GeV}$ to $1.5 \times 10^{15}\,{\rm GeV}$ when we vary x from 0.97 to 0 in the mean time for the standard embedding. If we choose the $M_{\rm GUT}$ to be $3 \times 10^{16}\,{\rm GeV}$, we obtain $M_{11} = 6.05 \times 10^{16}\,{\rm GeV}$, $x_{\rm lb} = -0.91$, $x_O = -0.826$, $x_{\rm H} = -0.758$, $[\pi\rho_{\rm p}]^{-1}$ goes from $2.64 \times 10^{15}\,{\rm GeV}$ to $5.2 \times 10^{15}\,{\rm GeV}$ when we vary x from 0.97 to 0 in the mean time. Also we notice that $x_{\rm lb}$, x_O, $x_{\rm H}$ increase if we increase the $M_{\rm GUT}$. Therefore, if we had a large GUT scale because of additional matter fields in the future M-theory model building, we might need to pay attention to $x_{\rm lb}$, x_O, $x_{\rm H}$ in order to get a clear picture of the universe.

Furthermore, we can discuss the possible low-energy scale of $[\pi\rho_{\rm p}]^{-1}$ which is interesting for the low-energy phenomenology when $x > 0$ for standard embedding. Let us define the relation between the physical Calabi–Yau manifold volume and the unification scale $M_{\rm GUT}$ as in [15]:

$$aM_{\rm GUT}^{-1} = (V_{\rm p}(1+x))^{1/6}, \tag{18}$$

where $a > 1$. a is smaller than 2.02 in order to keep $M_{\rm GUT} < M_{11}$ if we take $\alpha_{\rm GUT} = 1/25$. The formula is similar to the one above except for the transformation $M_{\rm GUT} \to M_{\rm GUT}/a$. Taking $M_{\rm GUT} = 2.0 \times 10^{16}\,{\rm GeV}$, $\alpha_{\rm GUT} = 1/25$, $M_{\rm Pl} = 2.4 \times 10^{18}\,{\rm GeV}$, we get the lower bound on $[\pi\rho_{\rm p}]^{-1}$: $9.5 \times 10^{13}\,{\rm GeV}$. Using $M_{\rm GUT} = 3.0 \times 10^{16}\,{\rm GeV}$, the lower bound is $3.2 \times 10^{14}\,{\rm GeV}$. It follows that $\Lambda_{\rm SUSY} \ge 10^{14}\,{\rm GeV}$, which is consistent with the estimate given in [15].

3 Soft terms

The Kähler potential, the gauge kinetic function and the superpotential in the simplest compactification of M-the-

ory on S^1/Z_2 are[2] [15,17]

$$K = \hat{K} + \tilde{K}|C|^2, \tag{19}$$

$$\hat{K} = -\ln[S+\bar{S}] - 3\ln[T+\bar{T}], \tag{20}$$

$$\tilde{K} = \left(\frac{3}{T+\bar{T}} + \frac{\alpha}{S+\bar{S}}\right)|C|^2, \tag{21}$$

$$\mathrm{Re}f^{O}_{\alpha\beta} = \mathrm{Re}(S+\alpha T)\delta_{\alpha\beta}, \tag{22}$$

$$\mathrm{Re}f^{\mathrm{H}}_{\alpha\beta} = \mathrm{Re}(S-\alpha T)\delta_{\alpha\beta}, \tag{23}$$

$$W = d_{xyz}C^xC^yC^z, \tag{24}$$

where S, T and C are dilaton, moduli and matter fields, respectively. α is a next order correction constant which is related to the Calabi–Yau manifold.

With this information, we have the following soft terms [14,19]:

$$M_{1/2} = \frac{\sqrt{3}M_{3/2}}{1+x}\left(\sin\theta + \frac{x}{\sqrt{3}}\cos\theta\right), \tag{25}$$

$$M_0^2 = M_{3/2}^2 - \frac{3M_{3/2}^2}{(3+x)^2}(x(6+x)\sin^2\theta + (3+2x)\cos^2\theta - 2\sqrt{3}x\sin\theta\cos\theta), \tag{26}$$

$$A = -\frac{\sqrt{3}M_{3/2}}{(3+x)}((3-2x)\sin\theta + \sqrt{3}x\cos\theta), \tag{27}$$

where $M_{3/2}$ is the gravitino mass; the quantity x defined above can also be expressed as

$$x = \frac{\alpha(T+\bar{T})}{S+\bar{S}}. \tag{28}$$

We pick the following two points as representatives which correspond to the scalar quasi-massless and the dilaton dominant scenario. The soft terms and parameters for the first point are

$$M_{1/2} = 0.989M_{3/2}, \quad M_0 = 0.008M_{3/2}, \tag{29}$$

$$A = -0.761M_{3/2}, \quad x = 0.5838, \quad \tan\theta = -4.566, \tag{30}$$

and the soft terms and parameters for the second one are

$$M_{1/2} = 1.534M_{3/2}, \quad M_0 = 0.870M_{3/2}, \tag{31}$$

$$A = -1.517M_{3/2}, \quad x = 0.13, \quad \theta = \frac{\pi}{2}. \tag{32}$$

[2] We choose this simplest case as an example. In fact, if we consider three families and three moduli, in order to avoid FCNC problems that might arise from the violation of the universal scalar masses in three families (although this kind of the violation might be very small), we might need to assume that $\alpha_1(T_1+\bar{T}_1) = \alpha_2(T_2+\bar{T}_2) = \alpha_3(T_3+\bar{T}_3)$, and $F^{T_1} = F^{T_2} = F^{T_3}$ where α_i $i = 1,2,3$ are the next order correction constants. Then, the final soft terms will be the same as the simplest case. So it is reasonable to choose the simplest case as an example to analyze the phenomenology

4 Mass spectra and the permitted parameter space

We concentrate on the two typical supersymmetry breaking (SB) scenarios given in Sect. 3 to calculate the low-energy spectrum of superpartner and Higgs bosons masses: the scalar quasi-massless scenario corresponding to $m_0 = 8.09\times10^{-4}M_{1/2}$ and $A = -0.769M_{1/2}$ (see (29), (30)) the dilaton dominant scenario corresponding to $m_0 = 0.567M_{1/2}$ and $A = -0.989M_{1/2}$ (see (31),(32)). In order to find the effects of the supersymmetry breaking scales to low-energy phenomenology, we take the supersymmetry breaking scales Λ_{SUSY} as 2.0×10^{16} GeV (the GUT scale), 1×10^{15} GeV, and 1×10^{14} GeV. The scales lower than 1×10^{14} GeV are not chosen because of the analysis in Sect. 2. But we will discuss their possible effects also. The other two free parameters, B and μ, in the M-inspired model are determined by the radiative breaking mechanism of the electroweak symmetry: one of them is traded off for $\tan\beta$, while for the other, only the freedom of sign remains [28,31]. Thus, there are only two free parameters, $M_{1/2}$ and $\tan\beta$, plus the sign of μ in our model.

We require that the lightest neutralino be the lightest supersymmetric particle (LSP) and use several experimental limits to constrain the parameter space, including

(1) the width of the decay $Z\to\chi_1^0\chi_1^0$ is less than 8.4 MeV, and the branching ratios of $Z\to\chi_1^0\chi_2^0$ and $Z\to\chi_2^0\chi_2^0$ are less than 2×10^{-5}, where χ_1^0 is the lightest neutralino and χ_2^0 is the other neutralino,
(2) the mass of the light neutral even Higgs cannot be lower than 77.7 GeV as the present experments required,
(3) the mass of the lighter chargino must be larger than 65.7 GeV as given by the Particle Data Group [29],
(4) sneutrinos are larger than 43.1 GeV,
(5) selectrons are larger than 58.0 GeV,
(6) smuons larger than 55.6 GeV, and
(7) staus larger than 45.0 GeV.

We use ISAJET to do numerical calculations. In order to include all effects of bottom and tau Yukawa couplings, we made some modifications to ISAJET which are the same as those in [30]. We first examine the $M_{1/2}$ dependence of sparticle and Higgs boson masses in the two SUSY breaking scenarios. It is found that the masses increase when $M_{1/2}$ increase and $M_{1/2}$ should not be larger than 400 GeV if one demands that the masses of superpartner and Higgs bosons are below 1 TeV. Then we scan the boundaries of the parameter space in the two scenarios, taking $M_{1/2}$ from zero to 400 GeV. For a certain scenario, as pointed out above, there are only two free parameters, $M_{1/2}$ and $\tan\beta$, as well as the sign of μ under the radiative electroweak symmetry breaking mechanism. The boundaries of the plane of the two parameters will be determined by the consistence conditions, such as that the input should naturally trigger electric–weak symmetry breaking, the gauge unification, the Yukawa couplings are in the perturbative range (no Yukawa coupling unification is imposed), and there should be no tachyonic particles in

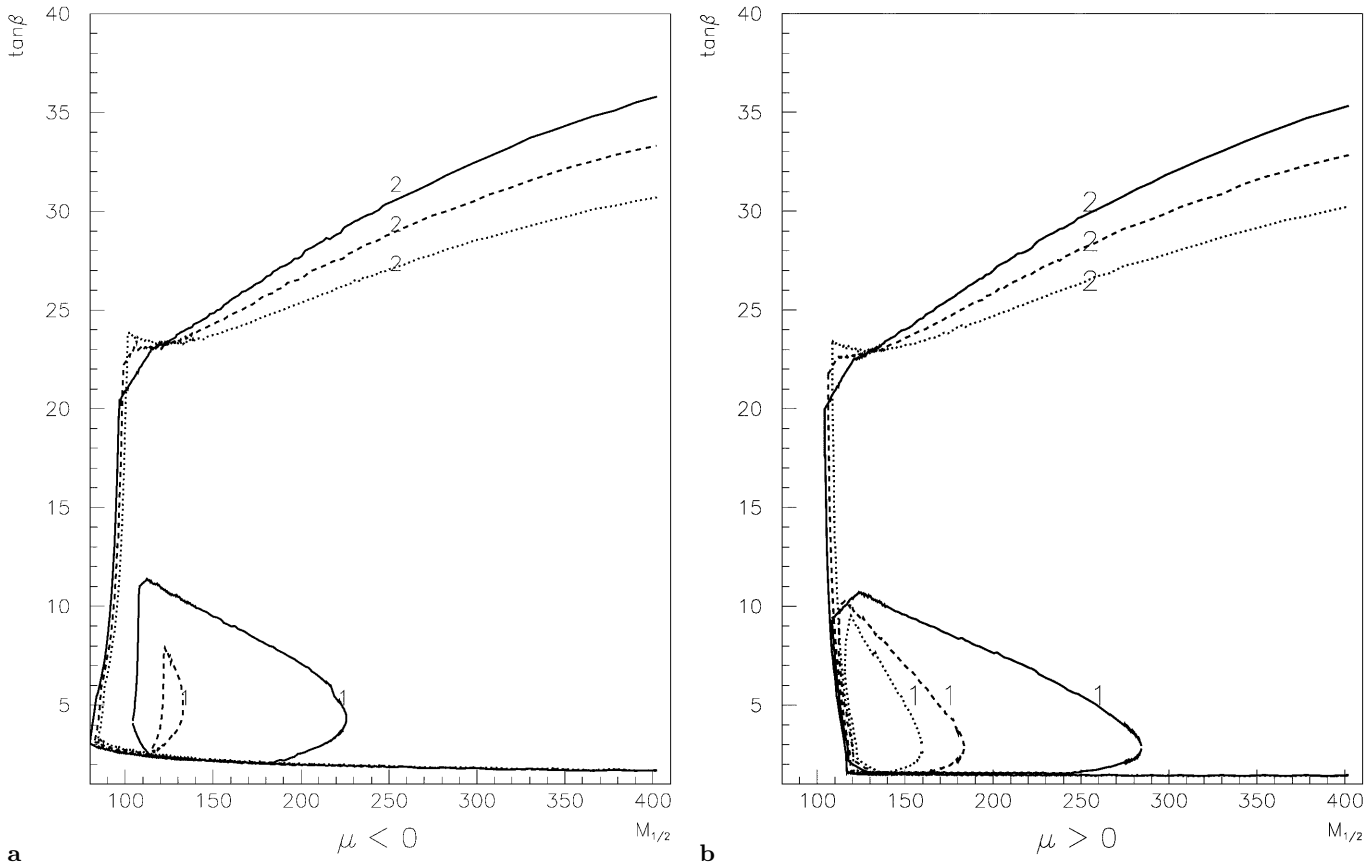

Fig. 1a,b. The upper and lower bounds of tanβ vary with $M_{1/2}$, for the dilaton dominant and scalar quasi-massless scenarios and for different values of $\Lambda_{\rm SUSY}$. The curve labeled 1 (2) represents the scalar quasi-massless (dilaton dominant) scenario. The dotted line is for $\Lambda_{\rm SUSY} = 10^{14}$ GeV, the dashed line 10^{15} GeV, and the solid line the GUT scale, 2×10^{16} GeV. For the scalar quasi-massless scenario, the permitted parameter spaces are with closed boundaries, while for the dilaton dominant scenario, the permitted parameter spaces are not closed in the right parts. **a** is for $\mu < 0$, **b** is for $\mu > 0$. The lower bound of tanβ is about 1.6 for the dilaton dominant scenario

the mass spectrum, and also we have the experimental limits listed above.

The results are shown in Fig. 1. The curves in Fig. 1 represent the upper bound and lower bound of tanβ for each $M_{1/2}$, for two different SB scenarios, and different $\Lambda_{\rm SUSY}$. Figure 1a shows the boundaries for $\mu < 0$, Fig. 1b for $\mu > 0$. The dotted line represents $\Lambda_{\rm SUSY}$ equals 10^{14} GeV, the dashed line 10^{15} GeV, and the solid line the GUT scale, 2.0×10^{16} GeV. The curves marked 1 (2) are the boundaries of the parameter spaces in the quasi-massless scenario (the dilaton dominant scenario). For the scalar quasi-massless scenario, the permitted parameter spaces are the areas enclosed with closed boundaries, while for the dilaton dominant scenario, the permitted parameter spaces are not closed in the right parts. The lower boundary of tanβ is about 1.6 for the dilaton dominant scenario. It is obvious from Fig. 1 that for the scalar quasi-massless scenario, the parameter space is tightly constrained to the low mass spectrum and there is no large tanβ region by consistence conditions, which is similar to what was found in [11,20], while for the dilaton dominant scenario there is a much larger parameter space allowed.

The effect of the sign of μ to the permitted parameter space is significant, as can be seen by comparing Figs. 1a and b. For example, in the scalar quasi-massless scenario and $\Lambda_{\rm SUSY}$=10^{14} GeV, if $\mu < 0$, the parameter space is completely excluded, while as $\mu > 0$, there does exist an allowed region. The shape of the boundaries of the parameter space for different signs of μ also agrees with this effect. But the effect in the dilaton dominant scenario is not as sensitive as in the quasi-massless scenario.

It is interesting that for the case of the dilaton dominant scenario and $\mu < 0$, the lower boundary of tanβ is singly determined by the experimental limit of the light Higgs mass. If the limit increases, the lower boundary will increase correspondingly. This may be understood from the tree level formula of the mass of the light Higgs, while the upper bound of tanβ is determined by both some experimental limits and the LSP condition. For example, when $\Lambda_{\rm SUSY}$ is 10^{14} GeV, $M_{1/2}$ from 84.7 GeV to 88.2 GeV, the upper bound is determined by the requirement that the mass M_Z of the Z^0 boson should be less than $2m_{\tilde{u}_l}$, $2m_{\tilde{e}_l}$, $2m_{\tilde{e}_r}$, $2m_{\tilde{\tau}_1}$, $2m_{\tilde{b}_1}$, and $2m_{\tilde{t}_1}$; from 88.2 GeV to 102.0 GeV, it is determined by $m_{\chi_1^\pm} > 65.7$

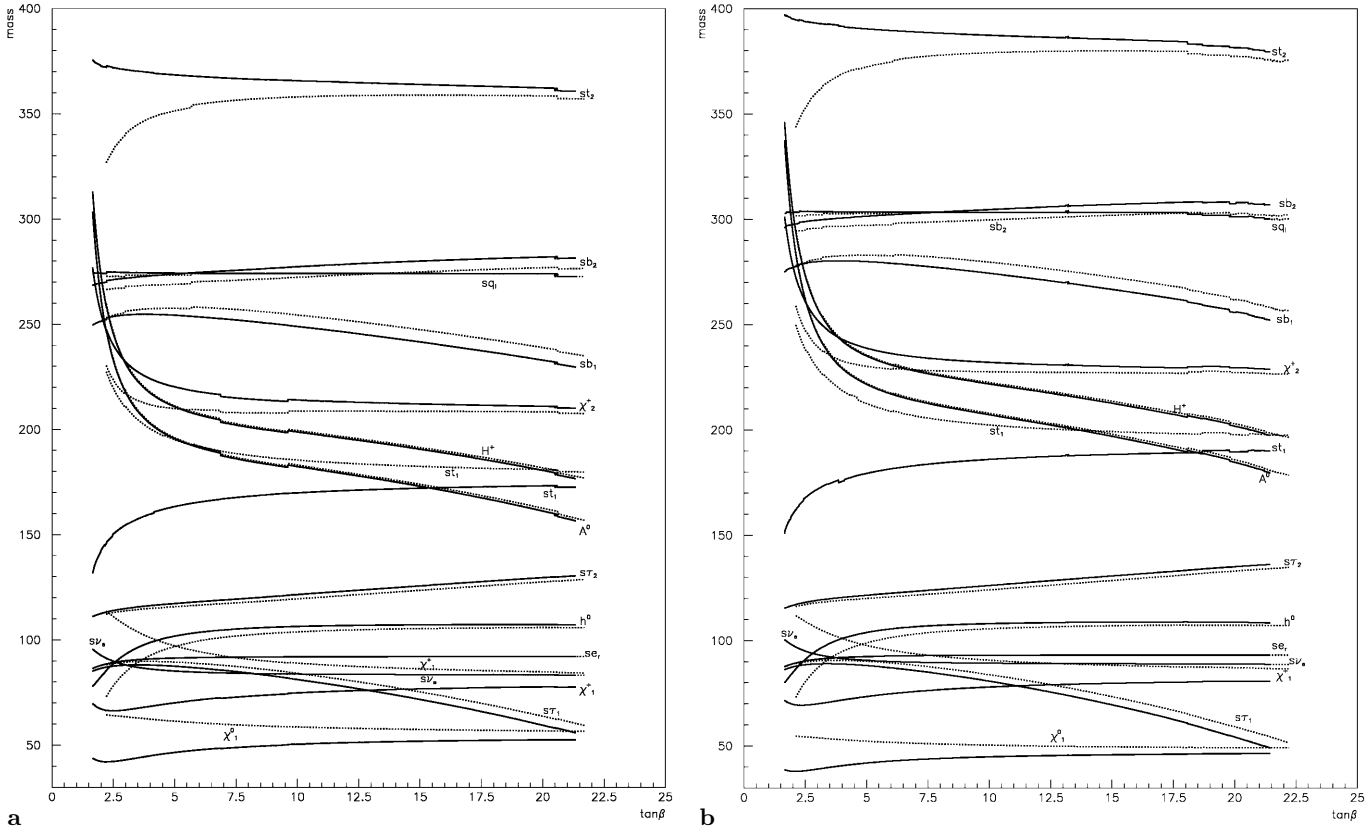

Fig. 2a,b. Computed values of super-particle masses versus tanβ for $M_{1/2} = 120\,\mathrm{GeV}$ in the dilaton scenario. **a** is for $\Lambda_{\mathrm{SUSY}} = 10^{14}\,\mathrm{GeV}$ and **b** $1 \times 10^{16}\,\mathrm{GeV}$. The solid (dashed) lines represent $\mu > (<)0$

GeV; from 102.0 GeV to 400 GeV by the LSP condition. The increase of the mass of the lighter chargino will generate a change of the upper limit of tanβ in the range, from about 85 GeV to 105 GeV, of $M_{1/2}$, but the change is not drastical. The numerical results are not sensitive to changes in the lower limits on masses of sneutrinos, selectrons, smuons and staus. That is, if using the up to date data on the masses instead of those used in the paper, Fig. 1 will not be changed.

An interesting aspect of the allowed parameter space of the dilaton dominant scenario is that there exists a region where the mass spectrum is low while tanβ is large. From Fig. 1, one obtains that the region increases when Λ_{SUSY} decreases in both the $\mu < 0$ and the $\mu > 0$ case. We find that if the bound of the lighter chargino mass increases, the region will be reduced. We know that $b \to s\gamma$ puts a very stringent constraint upon the parameter space of the MSSM. In this region, the charged Higgs mass is about 150 GeV and consequently it will lead to a significant contribution to $b \to s\gamma$. Therefore we would like to ask whether such a region can pass the constraint of $b \to s\gamma$. We will answer this question in the next section.

We illustrate the tanβ dependence of the mass spectra in the dilaton dominant scenario in Fig. 2, where we have chosen $M_{1/2} = 120\,\mathrm{GeV}$. We have chosen this value of $M_{1/2}$ because it is in the region of the parameter space pointed out above and, as noticed in [30], a study of this point serves to nicely illustrate the importance of large tanβ effects on Tevatron signals. The spectra are drawn in the same graph for $\mu > 0$ and $\mu < 0$ denoted by solid and dashed lines, respectively. In Fig. 2a, the supersymmetry breaking scale is 10^{14} GeV, while in Fig. 2b, the scale is 1×10^{16} GeV. It is apparent that the mass spectrum will drop with the decrease of Λ_{SUSY}, just as given in [11], because the mass spectra depend on the length of the running scale of the soft terms. The shorter the length, the lower the mass spectrum. This relation between the length of the running scale and mass spectra will keep till the Λ_{SUSY} is lower than 10^9 GeV. It is evident from Fig. 2 that the sign of μ can affect the spectrum, though not significantly. It is also manifest from the figure that the upper bound of tanβ is given by the LSP condition. The figure vividly shows the competition between the lightest neutralino and light stau for the LSP position. Another property worthy of mention is that most sparticles are insensitive to tanβ when tanβ is large except $m_{\tilde{\tau}_1}$ m_{A^0} and $m_{H^\pm}$.

5 Constraints from $b \to s\gamma$

It is well known that $b \to s\gamma$ put a very stringent constraint on the parameter space of various models [33,34]. In this section we analyze the constraints from $b \to s\gamma$

on the permitted parameter space discussed in the last section.

Five different sets of contributions to the decay $b \to s\gamma$ are present in supersymmetry. These can be classified according to the virtual particles exchanged in the loop:

(a) the SM contribution with exchange of W^- and up-quarks;
(b) the charged Higgs boson contribution with H^- and up-quarks;
(c) the chargino contribution with $\widetilde{\chi}^-$ and up-squarks ($\widetilde{u}$);
(d) the gluino contribution with $\tilde{g}$ and down-squarks ($\widetilde{d}$); and finally
(e) the neutralino contribution with $\widetilde{\chi}^0$ and down-squarks.

As pointed out in [48,31], contributions from neutrilino-down type squark (e) and gluino-down type squark (d) loop diagrams are, in general, negligible compared to those from chargino-up type squark diagrams because the flavor mixings between the third and the other two generations are small in minimal supergravity and constrained MSSM. However, in the large tanβ case, as shown in [35, 34], the gluino contribution can compete with the charged Higgs contribution in some regions of parameter space in mSUGRA where the lighter sbottom is light and the gluino mass is not large. In our model the two types of spectra are different from those in [35] and the regions in which we do the analysis are different from those in which the gluino contribution is important. Actually, in the region we considered, the mass of the lighter sbottom is about 230 GeV and the gluino mass is larger than 350 GeV so that the gluino contribution is not important, as can be seen from Fig. 11 in [35]. Moreover, in this region the mass of charged Higgs boson is equal to 150 GeV so that its contribution is significant. It seems that the gluino contribution might still not be important in our case. Although the neutralino contribution can increase for large tanβ, it does not remain big enough to compete with those from charged Higgs and SM [35]. Therefore, in addition to the contributions from SM and charged Higgs bosons, we only include the contributions from chargino-up type squark loop diagrams and call them SUSY contributions for the sake of simplicity in this paper. A detailed analysis of the gluino contributions in our model is needed and will be written down elsewhere.

It is known since long ago that a supersymmetric contribution can interfere either constructively or destructively [36–40], which is determined by the sign of μ. For $\mu < 0$, the SUSY contribution interferes destructively with the Higgs's and W's contributions. With the spectrum of sparticles low, both charged Higgs and supersymmetric particles can largely contribute to the process. So even if the charged Higgs has large contributions, the supersymmetric contribution will cancel its effect and, for large tanβ, can even overwhelm its and W's contributions and force the C_7 (C_7 is the Wilson coefficient of the operator O_7 in the effective Hamiltonian, (33), and the branching ratio of $b \to s\gamma$ is determined by $|C_7|^2$) to change sign from positive to negative while keeping the branch ratio still safely in the bounds of experiments.

As we pointed out in the last section, there exists a region where the mass spectrum is low while tanβ is large. It is known that a supersymmetric contribution is proportional to tanβ in this region. So it is expected that in this region the supersymmetric contribution will be very large.

Figure 3 shows the $b \to s\gamma$ constraint. The curves in Fig. 3a which have a dip correspond to the upper limit of tanβ, while the other ones correspond to the lower limit of tanβ. The curves in Fig. 3b which have a convex shape correspond to the upper limit of tanβ, while the other ones correspond to the lower limit of tanβ. The experimental bounds of $b \to s\gamma$ are translated into the bounds of C_7, denoted by the two solid horizontal lines. But it should be recalled that C_7 can be either negative or positive. So we map the allowed parameter space into the plane of $M_{1/2}$ and C_7. Because there is a large uncertainty (about $\pm 25\%$) in the leading order (LO) calculation of the $b \to s\gamma$ branching ratio we draw in the Fig. 3 two dashed horizontal lines corresponding to $|C_7|(1 + 0.3)$ and $|C_7|(1 - 0.3)$, respectively, in order to take the theoretical uncertainty into account. Figure 3a is for $\mu < 0$. It is apparent that for $\Lambda_{\rm SUSY} = 2 \times 10^{16}$ GeV if the theoretical error is kept into account the allowed region of the quasi-massless scenario can safely pass the experimental constraint due to the cancellation of the supersymmetric contribution to that of charged Higgs bosons when tanβ increases as shown by the line corresponding to the upper limit of tanβ. For the dilaton dominant scenario and $\Lambda_{\rm SUSY}$ equal to 2×10^{16} GeV, we can see from Fig. 3a that a quite large region is outside the experimental bound even if keeping the theoretical uncertainty into account. This is because in this region the SUSY contribution is not large enough to make C_7 still in the experimental bound after cancelling out contributions of the charged Higgs and W bosons. For the case of $\Lambda_{\rm SUSY}=10^{14}$ GeV, one can see from Fig. 3a that there is a region where the supersymmetric contribution indeed overwhelms the charged Higgs's and W's contributions and makes C_7 change sign. In this region tanβ is large and the mass spectrum is low. This region has an interesting phenomenology which has been analyzed in [30–32, 41, 42] and we shall discuss it in the next section. Recently, in order to make a more precise theoretical prediction, much literature was devoted to NLO corrections of this process [43–45]. It would be interesting to extend the analysis in this paper to include NLO corrections.

Figure 3b is devoted to $\mu > 0$. It is known that in such a case the supersymmetric contribution interferes constructively. But there still exists a small tanβ region for both scenarios in which the constraint from $b \to s\gamma$ can be satisfied within the theoretical uncertainty. One can see from the figure that for the dilaton dominant scenario, almost all of the large tanβ region is excluded by the $b \to s\gamma$ constraint.

For the dilaton dominant scenario and $\mu < 0$, it is possible to distinguish the interesting region where the mass spectrum is low and tanβ is large from the region where the mass spectrum and tanβ both are large. We shall discuss this possibility in an analysis of the rare decay $b \to s\tau^+\tau^-$.

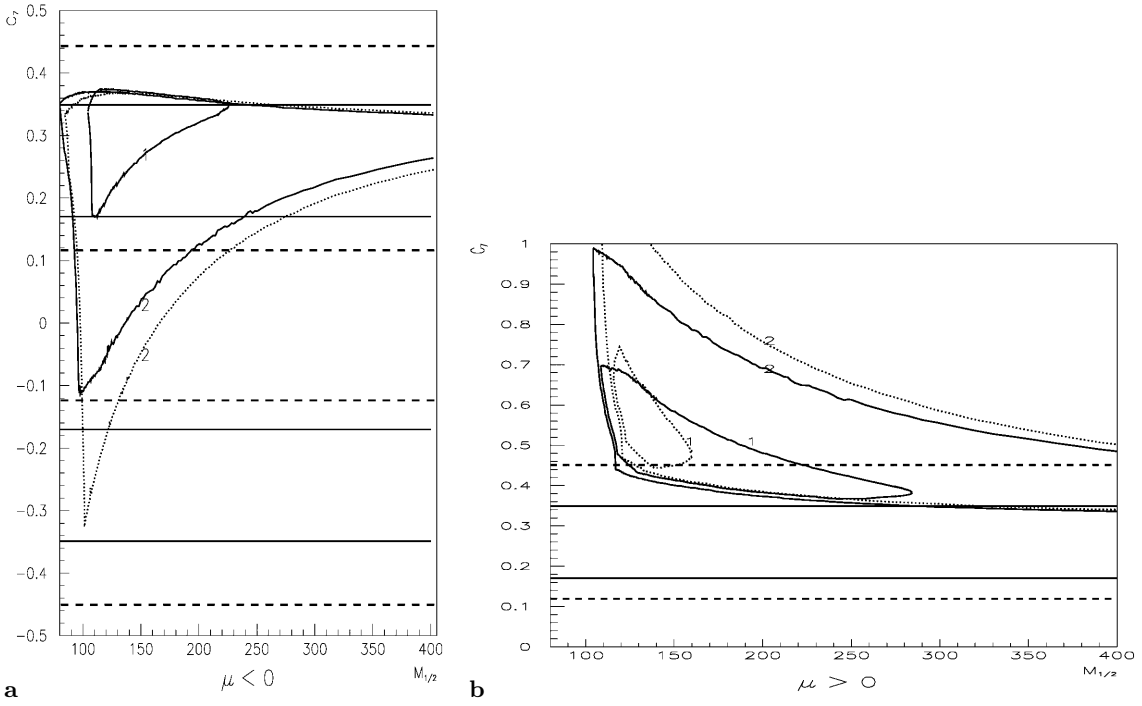

Fig. 3a,b. The variation of C_7 with $M_{1/2}$ and $\tan\beta$, scenarios and $\Lambda_{\rm SUSY}$. The solid lines represent $\Lambda_{\rm SUSY} = 2 \times 10^{16}$ GeV, the dotted lines represent $\Lambda_{\rm SUSY} = 1 \times 10^{14}$ GeV. The curve labeled 1 (2) represents the scalar quasi-massless (dilaton dominant) scenario. **a** is for the case $\mu < 0$, **b** for the case $\mu > 0$. The experimental constraint of $b \to s\gamma$ has been translated to the constraint on C_7, which is represented by two sets of solid horizontal lines and two sets of dashed horizontal lines. The solid lines correspond to the LO values of C_7 and the dashed ones to the values with which 30% theoretical error of the LO calculation has been taken into account. The curves in **a** which have a dip correspond to the upper limit of $\tan\beta$, while the other ones correspond to the lower limit of $\tan\beta$. The curves in **b** which have a convex shape correspond to the upper limit of $\tan\beta$, while the other ones correspond to the lower limit of $\tan\beta$

6 Some phenomenological predictions

We now proceed to the analysis of low-energy phenomenology. We shall discuss the rare decay $b \to s\tau^+\tau^-$ and Higgs boson productions $e^+e^- \to b\bar{b}H$. In order to search significant SUSY effects we shall concentrate on the case of the dilaton dominant scenario and $\mu < 0$.

6.1 Decay $b \to s\tau^+\tau^-$

The effective Hamiltonian relevant to the $b \to sl^+l^-$ process is

$$H_{\rm eff} = \frac{4G_F}{\sqrt{2}} V_{tb}V_{ts}^* \left(\sum_{i=1}^{10} C_i(\mu)O_i(\mu) + \sum_{i=1}^{10} C_{Q_i}(\mu)Q_i(\mu) \right) \tag{33}$$

where O_i $(i = 1, 2, \ldots, 10)$ are given in [46], and the Q_i's come from exchanging neutral Higgs bosons and have been given in [47]. The coefficients $C_i(m_w)$ and $C_{Q_i}(m_w)$ in SUSY models have been calculated [48–50,31,32]. The formulas of the invariant mass distribution and the backward-forward (B–F) asymmetry for $b \to s\tau^+\tau^-$ in the large $\tan\beta$ case have been given in[3] [31,47]. The branching ratio and B–F asymmetry depend on the coefficients C_7, C_8, C_9, C_{Q_1} and C_{Q_2}.

As was pointed out in [31,32], once C_{Q_1} and C_{Q_2} can compete with C_8 and C_9, both the invariant mass distribution and the backward–forward asymmetry will be greatly modified. The values of C_{Q_1} and C_{Q_2} depend on the mass splitting and the mixing angle of stops, the masses of charginos and diagonalizing matrices U and V, the masses of neutral Higgs bosons, and $\tan^3\beta$ when $\tan\beta$ is large. For small masses of the light chargino and neutral Higgs boson, there are large mass splitting of the stops and large $\tan\beta$, and C_{Q_1} and C_{Q_2} can be very large.

It is noted in the last section that, in the case of the dilaton dominant scenario, $\mu < 0$ and $\Lambda_{\rm SUSY}$=10^{14} GeV, after taking into account the constraint of $b \to s\gamma$, there does exist a region (we shall call it region A) of the parameter space where the masses of the sparticles are lower and $\tan\beta$ can go up to 25. In Fig. 4, we map the allowed parameter space into the C_{Q_1} and $M_{1/2}$ plane and the C_{Q_2} and $M_{1/2}$ plane, respectively. The lower boundary of $\tan\beta$ corresponds to the line near the $M_{1/2}$-axis, while the upper boundary corresponds to the other line. It is obvious that the values of C_{Q_1} and C_{Q_2} indeed are very large in this region. We choose $M_{1/2} = 110$ GeV and $\tan\beta = 23$ as a representative point in the region and the values of C_{Q_i} $(i = 1, 2)$ as well as C_i $(i = 7, 8, 9)$ at the point are

[3] For the earlier references on $b \to s\tau^+\tau^-$, see, for example, the references in [47]

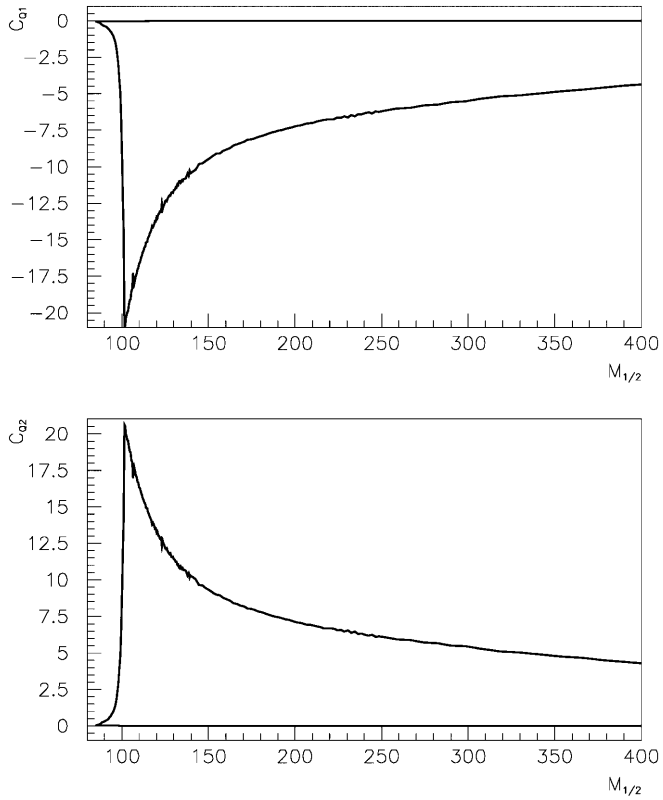

Fig. 4. For the case of the dilaton dominant scenario, $\mu < 0$ and $\Lambda_{\rm SUSY} = 10^{14}\,{\rm GeV}$, the variation of C_{Q_1} and C_{Q_2} with $M_{1/2}$ and $\tan\beta$. We map the permitted parameter space plane into the C_{Q_i} and $M_{1/2}$ planes. The lower boundary of $\tan\beta$ corresponds to the line near the $M_{1/2}$-axis, while the upper boundary corresponds to the other line

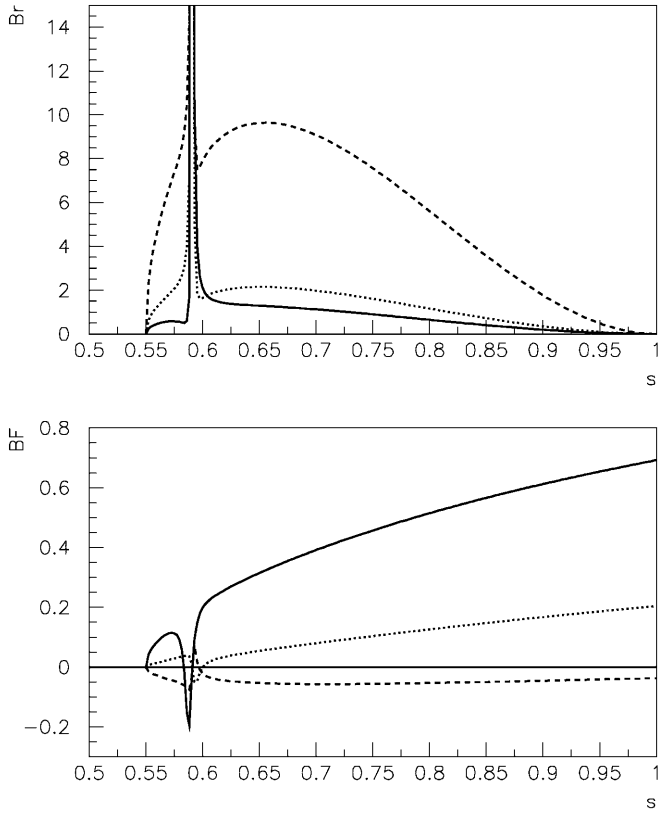

Fig. 5. The invariant mass distribution of the dilepton and B–F asymmetry for the process $b \to s\tau^+\tau^-$. The related coefficients and masses are listed in Tables 1 and 2, respectively. The solid line is for the SM prediction, the dashed line corresponds to the prediction of set A, the dotted line to the prediction of set B. We find that without including the contributions of neutral Higgs bosons, the deviation from SM is small

tabulated in Table 1. It is also noticed in the last section that there is another region (we shall call it region B) in the allowed parameter space where the mass spectrum and $\tan\beta$ both are large. In region B, because $\tan\beta$ can be up to 33, C_{Q_1} and C_{Q_2} can also compete with C_8 and C_9. But the values of C_{Q_1} and C_{Q_2} in this region are smaller when compared with those in region A. In order to distinguish this region from region A we have chosen $M_{1/2} = 400\,{\rm GeV}$ and $\tan\beta = 31$ as a representative in this region to do calculations. The values of C_{Q_i} $(i = 1, 2)$ and C_i $(i = 7, 8, 9)$ at the point are also tabulated in Table 1. One can see from this table that a typical C_{Q_1} in region A is -16, while a typical C_{Q_1} in region B is -4.5. Some masses of sparticles used in computations are listed in Table 2.

The numerical results of the invariant mass distribution and the B–F asymmetry for the two sets of values of coefficients C_{Q_i} and C_i given in Table 1 are shown in Fig. 5. It is obvious that the deviation from SM is very large for both cases, but for set A the deviation is more drastic. The enhancement of the differential branching ratio ${\rm d}\Gamma/{\rm d}s$ in the case of set A can reach 300% compared to SM. Meanwhile,the difference between set A and set B is also very significant so that one can distinguish them from the measurements of $b \to s\tau^+\tau^-$. It should be noted that without including the contributions of the neutral Higgs, the deviation from SM is small.

6.2 $e^+e^- \to b\bar{b}H$

The Higgs boson is the missing piece and also the least known of the standard model and supersymmetrical models. The pursuit of the Higgs bosons predicted by these models is one of the primary goals of the present and next generation of colliders. The Next Linear Collider (NLC) operating at a center-of-mass energy of 500–2000 GeV with a luminosity of the order of $10^{33}\,{\rm cm}^{-2}\,{\rm s}^{-1}$ may provide an ideal place to search for the Higgs bosons, since the events would be much cleaner than in the LHC and the parameters of the Higgs bosons would be easier to extract.

Based on the analysis in previous sections, we will present some data examples of the cross sections for the process $e^+e^- \to b\bar{b}H$ in this subsection. In Fig. 6 we show the SM Higgs production cross section as a function of the Higgs mass. In Figs. 7 and 8, we show the production cross sections as a function of $\tan\beta$, where $M_{1/2} = 120\,{\rm GeV}$ and 400 GeV, respectively, and the other param-

Table 1. The values of C_{Q_i} $(i = 1, 2)$ and C_i $(i = 7, 8, 9)$ for the chosen representative points in the regions A and B

	$M_{1/2}$	$\tan\beta$	C_7	C_8	C_9	C_{Q_1}	C_{Q_2}	BR$(b \to s\gamma)$
Set A	110	23	-0.25	-3.08	4.12	-16.64	16.36	2.14×10^{-4}
Set B	400	31	0.24	-3.06	4.50	-4.35	4.30	2.0×10^{-4}

Table 2. The masses of sparticles used in the computations for the chosen representative points in region A and B

	$m_{\tilde{q}}$	$m_{\tilde{t}_1}$	$m_{\tilde{t}_2}$	m_{χ_1}	m_{χ_2}	m_{h_0}	$m_{H^\pm}$	$m_{\tilde{\tau}_1}$	$m_{\chi_1^0}$
Set A	246.30	162.95	336.86	73.58	192.56	103.13	153.31	50.18	50.16
Set B	797.60	575.75	784.00	332.08	512.48	116.68	464.21	206.67	206.60

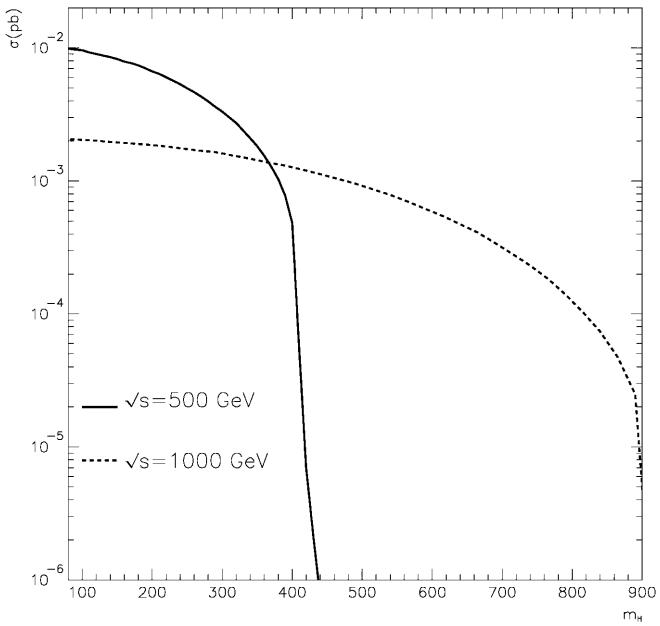

Fig. 6. The cross sections of the process $e^+e^- \to b\bar{b}H$ as a function of the mass of the SM Higgs boson $m_{\rm H}$

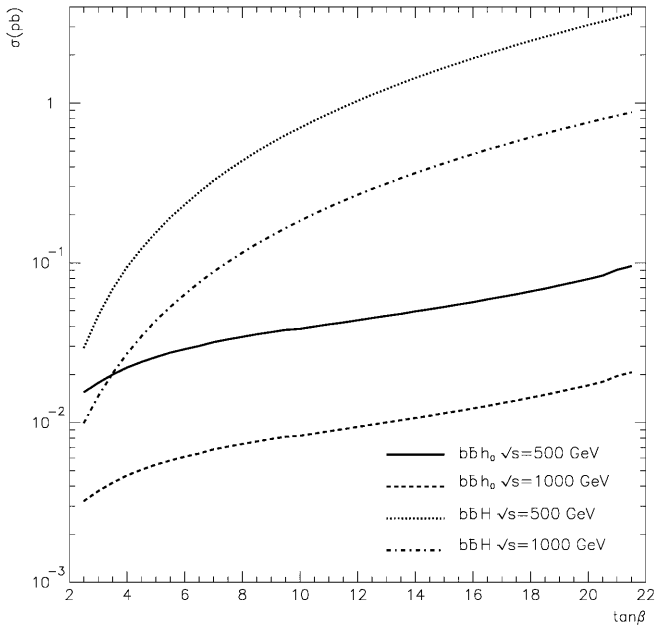

Fig. 7. The cross sections of the process $e^+e^- \to b\bar{b}H$ $(H = h^0, H^0)$ as a function of $\tan\beta$, where $M_{1/2} = 120\,\text{GeV}$, $\Lambda_{\rm SUSY} = 10^{14}\,\text{GeV}$ and $\text{Sign}(\mu) = -1$ in the dilaton dominant scenario

eters are depicted in the figure captions. As usual, h^0 and H^0 denote the CP-even neutral Higgs bosons with $m_{h^0} < m_{H^0}$, respectively. It should be noticed that, as $M_{1/2} = 400\,\text{GeV}$, the mass of H^0 is too heavy to be produced by the NLC when $s^{1/2} = 500\,\text{GeV}$. Comparing Figs. 7 and 8 with Fig. 6, it is evident that the Higgs production cross sections increase significantly when $\tan\beta$ increases, as expected, except for $b\bar{b}h^0$ in the case of $M_{1/2} = 400\,\text{GeV}$. For the $b\bar{b}h^0$ production, the enhancement of large $\tan\beta$ is offset by the small $\sin\alpha$ because in the case of $M_{1/2} = 400\,\text{GeV}$, m_{h^0} is much smaller than the masses of the other Higgs bosons.

7 Conclusions

We have reconsidered the 11-dimensional Planck scale, the physical scale of the eleventh dimension, the physical scale of the Calabi–Yau manifold and the coupling in the hidden sector in M-theory on S^1/Z_2 and discussed reasonable bounds on them with the ansatz that the scale of $M_{\rm GUT}$, $M_{\rm H}$ and $[\pi\rho_{\rm p}]^{-1}$ should be lower than the dimension-11 Planck scale. It has been shown that $\Lambda_{\rm SUSY} \geq 10^{14}\,\text{GeV}$ if one assumes $\Lambda_{\rm SUSY} = [\pi\rho_{\rm p}]^{-1}$ [11]. Choosing two representative points which correspond to the scalar quasi-massless scenario and dilaton dominant SUSY breaking scenario, respectively, we have calculated the sparticle spectra at different values of $\Lambda_{\rm SUSY}$ and found that the spectra are lower when $\Lambda_{\rm SUSY}$ decrease. Therefore, compared with the spectra in the weakly coupling string models and general SUSY GUT models, the spectra in M-theory phenomenology are lower, which is, of course, easier to search at colliders. The LEP experiments and the $b \to s\gamma$ constraint on the parameter space in the dilaton dominant and scalar quasi-massless supersymmetry

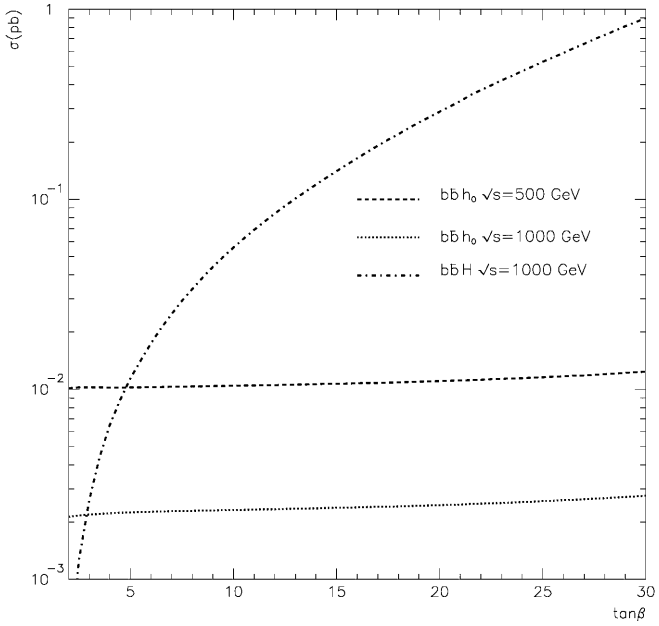

Fig. 8. Same as Fig. 7 but $M_{1/2} = 400\,\mathrm{GeV}$

breaking scenarios are analyzed. Finally, we give predictions for the rare decay $b \to s\tau^+\tau^-$ and neutral Higgs boson productions. An interesting result is that one could discover supersymmetry from $b \to s\tau^+\tau^-$ in B factories if nature gave us a large $\tan\beta$ and low mass spectra which come out as a consequence of M-theory low-energy phenomenology.

Acknowledgements. This research was supported in part by the National Science Foundation of China. The research by T. Li was supported in part by the U.S. Department of Energy under Grant No. DE-FG02-95ER40896 and in part by the University of Wisconsin Research Committee with funds granted by the Wisconsin Alumni Research Foundation. This work was also supported in part by the post doctoral foundation of China and S.-H. Zhu gratefully acknowledges the support of K.C. Wong Education Foundation, Hong Kong.

References

1. For reviews see: J.H. Schwarz, Nucl. Phys. Proc. Suppl. B **55**, 1 (1997); M.J. Duff, Int. J. Mod. Phys. A **11**, 5623 (1996); Fields, Strings, and Duality (TASI 96), edited by C. Efthimiou, B. Greene (World Scientific, 1997)
2. P. Horava, E. Witten, Nucl. Phys. B **475**, 94 (1996)
3. E. Witten, Nucl. Phys. B **471**, 135 (1996)
4. P. Horava, Phys. Rev. D **54**, 7561 (1996)
5. T. Banks, M. Dine, Nucl. Phys. B **479**, 173 (1996); hep-th/9609046
6. K. Choi, Phys. Rev. D **56**, 6588 (1997); K. Choi, H.B. Kim, H. Kim, hep-th/9808122
7. I. Antoniadis, M. Quiros, Phys. Lett. B **392**, 61 (1997)
8. I. Antoniadis, M. Quiros, hep-th/9705037, hep-th/9707208, hep-th/9709023
9. E. Dudas, J.C. Grojean, hep-th/9704177; E. Dudas, hep-th/9709043
10. E. Caceres, V.S. Kaplunovsky, I.M. Mandelberg, Nucl. Phys. B **493**, 73 (1997)
11. T. Li, J.L. Lopez, D.V. Nanopoulos, hep-ph/9702237, Mod. Phys. Lett. A **12**, 2647 (1997)
12. T. Li, J.L. Lopez, D.V. Nanopoulos, Phys. Rev. D **56**, 2602 (1997)
13. T. Li, Phys. Rev. D **57**, 7539 (1998)
14. T. Li, Phys. Rev. D **59**, 107902 (1999)
15. H.P. Nilles, M. Olechowski, M. Yamaguchi, hep-th/9707143, Phys. Lett. B **415**, 24 (1997); hep-th/9801030
16. Z. Lalak, S. Thomas, hep-th/9707223
17. A. Lukas, B.A. Ovrut, D. Waldram, hep-th/9710208, hep-th/9803235
18. A. Lukas, B.A. Ovrut, D. Waldram, hep-th/9711197
19. K. Choi, H.B. Kim, C. Munoz, hep-th/9711158
20. D. Bailin, G.V. Kraniotis, A. Love, hep-ph/9803274
21. J. Ellis, A.E. Faraggi, D.V. Nanopolous, hep-th/9709049
22. E. Dudas, J. Mourad, hep-th/9701048
23. K. Benakli, hep-th/9805181
24. S. Stieberger, CERN-TH-98-228 (Jul 1998) 34p. [HEP-TH 9807124] to appear in Nucl. Phys. B
25. Z. Lalak, S. Pokorski, S. Thomas, hep-ph/9807503
26. A. Lukas, B.A. Ovrut, D. Waldram, hep-th/9808101
27. D.V. Nanopolous, hep-th/9711080
28. K. Inoue, A. Kakuto, H. Komatsu, S. Takeshita, Prog. Theor. Phys. **68**, 927 (1982); ibid, **71**, 413 (1984); L. Ibáñez, G.G. Ross, Phys. Lett. B **110**, 215 (1982); L. Alvarez-Gaumé, J. Polchinski, M.B. Wise, Nucl. Phys. B**221**, 495 (1983); J. Ellis, J.S. Hagelin, D.V. Nanopoulos, K. Tamvakis, Phys. Lett. B **125**, 275 (1983)
29. Particle Data Group, Review of Particle Properties, Eur. Phys. J. C **3**, 1 (1998)
30. H. Baer, C.-H. Chen, M. Drees, F. Paige, X. Tata, Phys. Rev. Lett. **79**, 986 (1997)
31. Chao-shang Huang, Qi-shu Yan, Phys. Lett. B **442**, 209 (1998)
32. Chao-shang Huang, Wei Liao, Qi-shu Yan, Phys. Rev. D **59**, 011701 (1999)
33. W. de Boer, H.-J. Grimm, A.V. Gladyshev, D.I. Kazakov, Phys. Lett. B **438**, 281 (1998); T. Goto, Y. Okada, Y. Shimizu, Phys. Rev. D **58**, 094006 (1998)
34. F. Borzumati, C. Greub, T. Hurth, D. Wyler, hep-ph/9911245 and references therein
35. F. Borzumati, Z. Phys. C **63**, 291 (1994)
36. J.L. Lopez, D.V. Nanopoulos, X. Wang, A. Zichichi, Phys. Rev. D **51**, 147 (1995)
37. R. Barbieri, G.F. Giudice, Phys. Lett. B **309**, 86 (1993)
38. M.A. Diaz, Phys. Lett. B **322**, 591 (1994)
39. T. Goto, Y. Okada, Prog. Theor. Phys. **94**, 407 (1995)
40. R. Garisto, J.N. Ng, Phys. Lett. B **315**, 372 (1993)
41. H. Baer, C.-H. Chen, M. Drees, F. Paige, X. Tata, hep-ph/9809223
42. W. Loinaz, J.D. Wells, hep-ph/9808287
43. M. Neubert, hep-ph/9809377
44. M. Ciuchini et al., hep-ph/9806308
45. A.L. Kagan, M. Neubert, hep-ph/9805303
46. B. Grinstein, M.J. Savage, M.B. Wise, Nucl. Phys. B **319**, 271 (1989)
47. Y.B. Dai, C.S. Huang, H.W. Huang, Phys. Lett. B **390**, 257 (1997)
48. S. Bertolini, F. Borzumati, A. Masieso, G. Ridolfi, Nucl. Phys. B **353**, 591 (1991)
49. P. Cho, M. Misiak, D. Wlyer, Phys. Rev. D **54**, 3329 (1996)
50. T. Goto, Y. Okada, Y. Shimizu, M. Tanaka, Phys. Rev. D **55**, 4273 (1997)